small

Direct Laser-Patterned Micro-Supercapacitors from Paintable MoS_2 Films

Liujun Cao, Shubin Yang, Wei Gao, Zheng Liu, Yongji Gong, Lulu Ma, Gang Shi, Sidong Lei, Yunhuai Zhang, Shengtao Zhang,* Robert Vajtai, and Pulickel M. Ajayan**

***M**icrometer-sized electrochemical capacitors have recently attracted attention due to their possible applications in micro-electronic devices. Here, a new approach to large-scale fabrication of high-capacitance, two-dimensional MoS_2 film-based micro-supercapacitors is demonstrated via simple and low-cost spray painting of MoS_2 nanosheets on Si/SiO_2 chip and subsequent laser patterning. The obtained micro-supercapacitors are well defined by ten interdigitated electrodes (five electrodes per polarity) with 4.5 mm length, 820 μm wide for each electrode, 200 μm spacing between two electrodes and the thickness of electrode is ~0.45 μm. The optimum MoS_2-based micro-supercapacitor exhibits excellent electrochemical performance for energy storage with aqueous electrolytes, with a high area capacitance of 8 mF cm^{-2} (volumetric capacitance of 178 F cm^{-3}) and excellent cyclic performance, superior to reported graphene-based micro-supercapacitors. This strategy could provide a good opportunity to develop various micro-/nanosized energy storage devices to satisfy the requirements of portable, flexible, and transparent micro-electronic devices.*

L. J. Cao, Dr. S. B. Yang, Dr. Z. Liu, L. L. Ma, G. Shi, S. D. Lei, Dr. R. Vajtai, Prof. P. M. Ajayan
Department of Mechanical Engineering & Materials Science
Rice University
Houston, Texas 77005, USA
E-mail: sy13@rice.edu; ajayan@rice.edu

L. J. Cao, Prof. Y. H. Zhang, Prof. S. T. Zhang
School of Chemistry and Chemical Engineering
Chongqing University
Chongqing 400044, China
E-mail: stzhang@cqu.edu.cn

Y. J. Gong, Prof. P. M. Ajayan
Department of Chemistry
Rice University
Houston, Texas 77005, USA

Dr. W. Gao
Los Alamos National Laboratory
Los Alamos, NM, 87545, USA

DOI: 10.1002/smll.201203164

1. Introduction

Micro-electrochemical capacitors are important complements to batteries due to their high power density.[1–3] To date, two kinds of capacitive behaviors have been observed in materials used as electrodes in micro-electrochemical capacitors based on their different energy storage mechanisms. One is the electrochemical double layer capacitance (EDLC) related to the double layer formation at the interfaces between electrolyte and electrode surface,[7] while the other is pseudo-capacitance related to the fast and reversible redox reactions occurring in the electrodes.[4,5] Very recently, various carbons including carbide-derived carbon,[6] activated carbon,[7] onion-like carbon,[8] carbon nanotubes[9–11] and graphene sheets (or reduced graphene oxide sheets)[12,13] have been widely used as electrode materials for EDLC based micro-sized or thin-film supercapacitors. In this regard, graphene is one of the most attractive materials due to its high surface area[15] and exceptional mechanical properties and high electrical conductivity.[14] Unfortunately,

the low area capacitance of graphene micro-devices[12] (0.5~3 mF cm^{-2}) based on EDLC partially hampers its broad use in high power applications.

MoS_2 nanosheets, a graphene-like 2D material, have shown unique structural and electronic properties.[16–19,29–35] In a single MoS_2 nanosheet, the Mo atomic layer is sandwiched between two sulfur layers *via* covalent bonding. And their multi-layers are stacked by van der Waals force, allowing easy intercalation of foreign ions (H^+, Li^+). More importantly, the center Mo atoms possess a range of oxidation states from +2 to +6, promising a typical pseudo-capacitance behavior with very high specific capacitance for MoS_2 nanosheets, similar to that of RuO_2, the theoretical capacitance ~1000 F g^{-1}. Moreover, several procedures such as hydrothermal processes,[20] intercalation-exfoliation method[21,22] and liquid phase exfoliation have been developed to prepare MoS_2 nanosheets in bulk quantities.[23,24] Combined with good fabrication technologies from nanosheets to films, MoS_2 nanosheets should be a promising pseudo-capacitance material for high performance micro-supercapacitors.

Here, we demonstrate a new approach for large-scale fabrication of 2D MoS_2 film based micro-supercapacitors *via* simple spray painting of MoS_2 nanosheets to form thin films and subsequent laser patterning. The resulting MoS_2 micro-supercapacitors are consisting of well-defined finger-like electrodes built from large number of curly MoS_2 nanosheets; the structure of the film facilitates the access of the ions to the electrode surface. The optimized micro-supercapacitor exhibits excellent electrochemical performances and energy storage using aqueous electrolytes, it has high area capacitance of 8 mF cm^{-2} and excellent cyclic performance, superior to reported graphene-based micro-supercapacitors.

2. Results and Discussion

As illustrated in **Figure 1**, 2D MoS_2 film based micro-supercapacitors were fabricated *via* laser patterning of painted MoS_2 films. First, two types of free-standing MoS_2 nanosheets were synthesized via an anionic sulfate surfactant assisted hydrothermal process and a liquid exfoliation approach; the as-prepared MoS_2 nanosheets were denoted as h-MoS_2 and e-MoS_2, respectively. Both of the MoS_2 nanosheet samples were then dispersed in mixed solutions of ethanol and water (ethanol/water volume rate = 4:1) to form inks for painting (for details, see Supporting Information). Subsequently, the stable suspensions were spray painted onto Si\SiO_2 wafers and MoS_2 films with uniform thickness were generated after the solvent evaporated (Figure 1A, steps 1 and 2). A finger-electrode pattern was defined by laser patterning (Figure 1A, step 3), and the obtained pattern electrode was assembled into an electrochemical test cell (Figure 1C). The photograph of a typical painted and patterned film (Figure 1B) shows a well-defined arrangement and the separation between the electrodes; the micro-device was constructed with 10 interdigitated electrodes (4.5 mm length, 820 μm wide for each electrode) with appropriate thickness (~0.45 μm, five electrodes

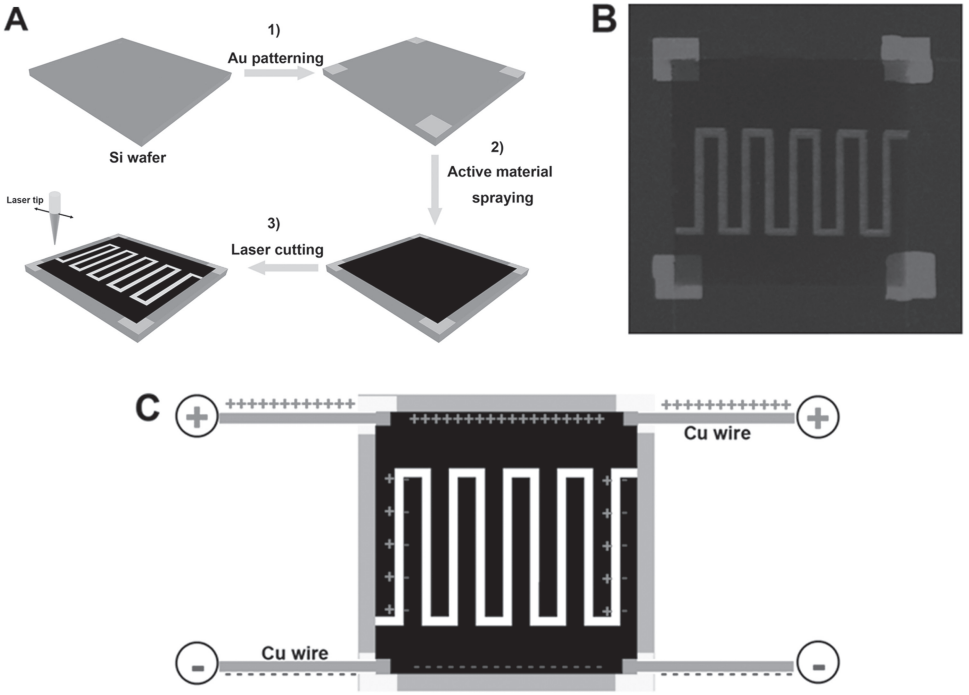

Figure 1. (A) Fabrication of MoS_2 film micro-supercapacitorsin three steps: 1) deposition of gold electrical conductive pads on the standard silicon chips for use as current collectors, 2) masking and spray painting MoS_2 ink on the chips, 3) patterning interdigitated finger electrodes (five electrodes per polarity) on the active material area by laser cutting process. (B) A typical photograph of the as-prepared MoS_2 film micro-supercapacitor. Each of the finger electrodes is 4.5 mm long, 820 μm wide and the spacing between two finger electrodes is 200 μm. (C) Top view of the electrochemical testing device. Cu wire was used for electrical contacts. The black area is the MoS_2 active material including patterned interdigitated finger electrodes and pads, and the white area between them is the separator which is filled with electrolyte during the electrochemical tests.

NANO MICRO small

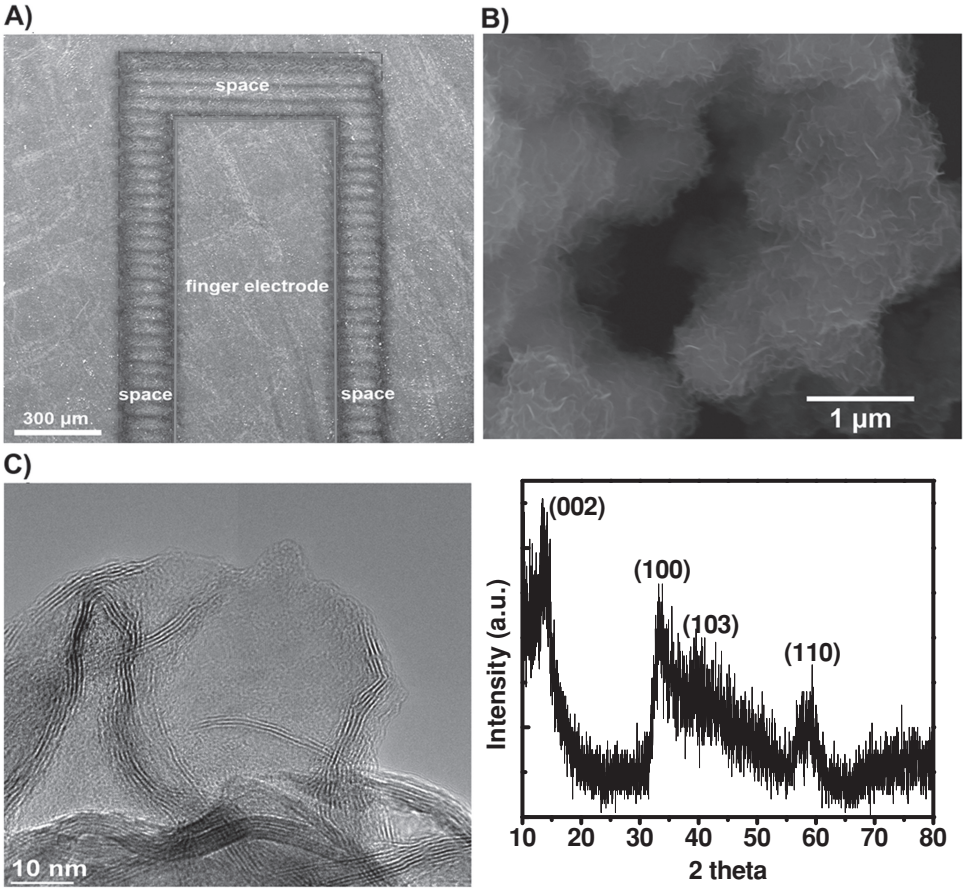

Figure 2. Characterization of representative h-MoS_2 finger electrodes and h-MoS_2 nanosheets. (A) Typical SEM image of a finger-like h-MoS_2 electrode (solid line area), the space was generated by laser cutting (dot line area). (B) SEM image of h-MoS_2 nanosheets that constructed the h-MoS_2 film micro-supercapacitor. (C) HRTEM image of h-MoS_2 nanosheets demonstrated to be 2~7 atomic layers. (D) X-ray diffraction (XRD) patterns of h-MoS_2 nanosheets.

per polarity (Figure S1 in Supporting Information). This structure of the device is demonstrated by the typical SEM image of one finger electrode in **Figure 2**(A), where the MoS_2 nanosheets are well controlled as a result of the patterning process (Figure S2). Note that such a simple strategy allows us to prepare various micro-electrodes without use of any organic binders. (For details, see Supporting Information).

The morphology and the crystalline structure of h-MoS_2 and e-MoS_2 nanosheets sprayed to form the MoS_2 film electrodes were investigated *via* scanning electron microscopy (SEM) and transmission electron microscopy (TEM). In case of h-MoS_2 nanosheets, crumpled morphology with layered structure is visible (Figure 2B and Figure S3 (A)), originating from the thinness of MoS_2 atomic layers. In contrast, the exfoliated MoS_2 nanosheets are more flat and rigid (Figure S4 (A)). The thickness of representative h-MoS_2 and e-MoS_2 nanosheets are demonstrated to be 2~7 and 1–3 atomic layers, respectively; the interlayer spacing is ~0.65 nm (Figure 2C and Figure S4 (C)). The high-resolution TEM (HRTEM) image also reveals the well-defined hexagonal crystalline lattice of both the h-MoS_2 and e-MoS_2 nanosheets (Figure S3 (B) and Figure S4 (B)). X-ray photoelectron survey scan spectra (XPS) reveals the presence of Mo and S with atomic ratio of 1:2, and no any impurites in both h-MoS_2 and e-MoS_2 samples. (Figure S5 (A)). The high-resolution Mo 3d XPS spectra can be deconvoluted into two peaks of signals with binding energies of 228.4 and 231.5 eV for both samples, corresponding to the doublet $Mo3d_{5/2}$ and $Mo3d_{3/2}$, respectively (Figure S5 (B,C)). The high resolution S2p XPS spectra also shows two binding energies of 162.4 and 161.3 eV (h-MoS_2), corresponding to $S2p_{1/2}$ and $S2p_{3/2}$, respectively (Figure S5 (D, E)). The crystalline structure of our MoS_2 nanosheets was further confirmed by the Raman spectra and X-ray diffraction (XRD) patterns. As it is shown in Figure S6, the Raman spectra have two peaks at ~381 and 406 cm^{-1} which are attributed to the A_{1g} and E_{2g} modes, respectively. The indexed XRD pattern is shown in Figure 2 (D), the peaks corresponding to the (100), (103), (110) planes are matching well the JCPDS card (37–1492). The weak (002) reflection indicates that the produced nanosheets are made of few layers assembled by van der Waals interactions (a spacing of 0.65 nm), in good agreement with the observation from TEM images.

The electrochemical performance of the as-prepared h-MoS_2 film based micro-supercapacitor was first studied by cyclic voltammetry (CV) at various scan rates over the voltage range of –0.5–0.5 V. As presented in **Figure 3**A and Figure S7 (see Supporting information), two hump peaks at

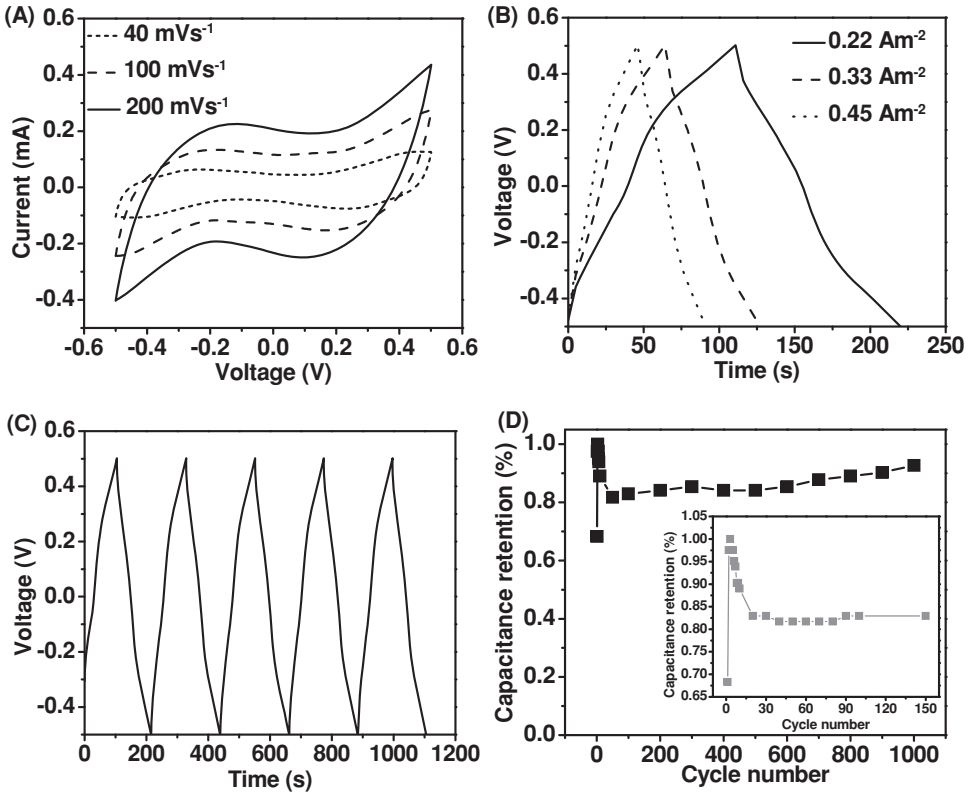

Figure 3. (A) CV curves of h-MoS_2 film based micro-supercapacitor at different scanning rates of 40, 100 and 200 mVs^{-1}. (B) Galvanostatic charge-discharge (GAL) curves of h-MoS_2 micro-supercapacitor at different current densities from 0.22 to 0.45 A m^{-2}. (C) Galvanostatic cycling behavior at a current density of 0.22 A m^{-2}. (D) Cycling performance of h-MoS_2 micro-supercapacitor over 1000 cycles at a current density of 0.22 Am^{-2}, the inset of (D) is the cycle performance for the first 150 cycles.

~0.2 and –0.2 V are observed. With increasing the scan rate from 10 to 200 mV s^{-1}, both peaks become more dominant owing to the strengthened redox reaction ($MoS_2+K^++e^-$ = MoS-SK^+), consistently with characteristics of MoS_2 electrodes in supercapcitors with aqueous electrolyte.[25] This pseudo-capacitance behavior of h-MoS_2 microsupercapacitor is further confirmed by the nonlinear galvanostatic charge-discharge curves at different current densities as shown in Figure 3B. A high area capacitance of 8 mF cm^{-2} is achieved at a scan rate of 10 mV s^{-1}, which is much higher than that reported for onion-like carbon- and graphene-based micro-supercapatictors (0.5~3 mF cm^{-2}).[8,12]

The cycle performance of h-MoS_2 film based microsupercapacitor was further examined by charge-discharge testing at a current density of 0.22 Am^{-2}. Remarkably enough, only ~8% of capacitance fades after 1,000 cycles, representing excellent cycle stability. The small capacitance fading in the first 150 cycles perhaps originates from the "active" sites saturation on the surface of MoS_2 film during the charge-discharge process, and the later capacitance increase should be attributed to the "intercalation" induced capacitance behavior caused by the intercalation of foreign ions (Na^+) into van der Waals gaps of multilayers of MoS_2. This phenomenon is similar to the one reported for most layered transition metal oxides (such as TiS_2, TiO_2 (B), MoO_3 etc) applied in energy storage.[3,26–28]

In comparison, the liquid exfoliated MoS_2 nanosheets (e-MoS_2) prepared from bulk MoS_2 and commercially available MoS_2 powders (size, <2 μm) were also employed for fabrication of MoS_2-based microsupercapacitors *via* the same procedures. (For details, see Supporting information). Apparently, the CV area of h-MoS_2 and e-MoS_2 is significantly higher than comparable bulk MoS_2 powder, indicating the higher capacitance for h-MoS_2 and e-MoS_2 based micro-supercapacitor (**Figure 4**A and Figure S7 and S8). This is further confirmed by their galvanostatic charge-discharge tests at a constant current density of 0.22 A m^{-2}. As presented in Figure 4B and Figure S6, the area capacitance of h-MoS_2 based micro-supercapacitor is 8 mF cm^{-2}, much higher than those of e-MoS_2 (~3.1 mF cm^{-2}) and MoS_2 powder (1.8 mF cm^{-2}). Correspondingly, the highest volumetric capacitance is 178 F cm^{-3} for h-MoS_2 based micro-supercapacitor, which is comparable to those reported for the best micro-supercapacitors (~180 F cm^{-3} in organic electrolyte and ~160 F cm^{-3} in aqueous electrolyte).[6] The superior electrochemical performance of h-MoS_2 film based microsupercapacitor should be attributed to the favorable structures of h-MoS_2 nanosheets for energy storage: (1) 2D graphene-like sheet structure, which maximizes the surface effects compared to bulk MoS_2 and restacked e-MoS_2 nanosheets, and provides a larger number of "active" sites for fast and reversible surface redox reactions; (2) rough morphology of MoS_2 layers, leading to a better pore structure for easy access of the ions from the aqueous electrolyte to the electrodes.

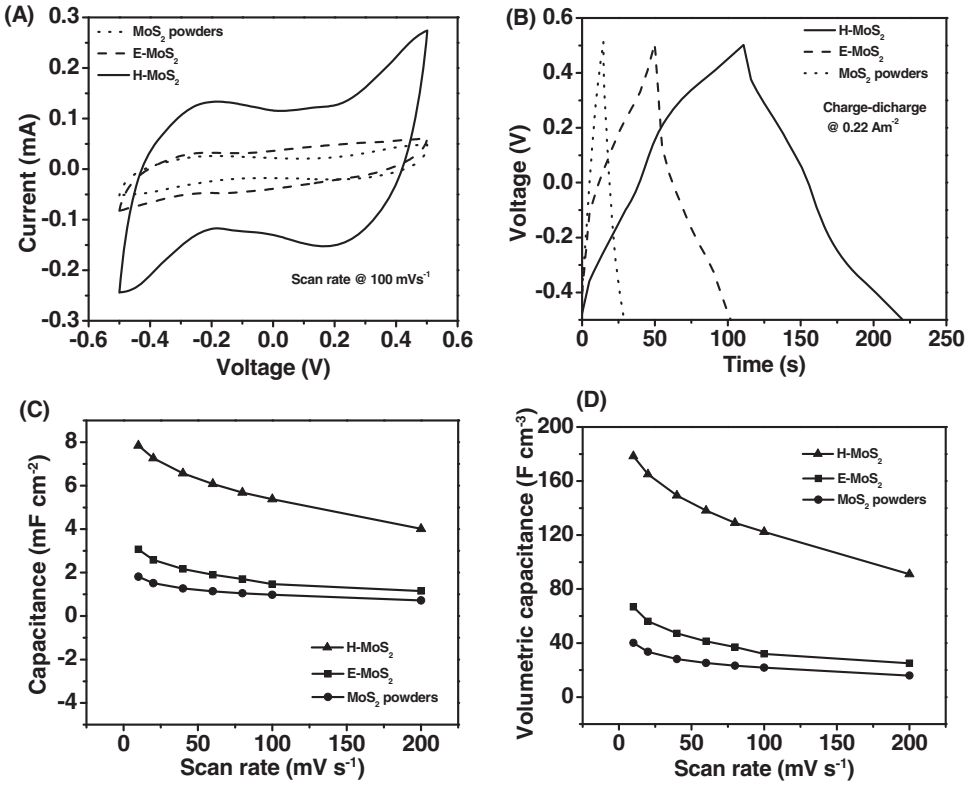

Figure 4. Comparison of the electrochemical performance of h-MoS_2 nanosheet, e-MoS_2 nanosheet and MoS_2 powder based micro-supercapacitors. (A) CV curves of h-MoS_2 nanosheet, e-MoS_2 nanosheet and MoS_2 powder based micro-supercapacitors at a scan rate of 100 mV s^{-1}. (B) Galvanostatic charge-discharge (GAL) of h-MoS_2 nanosheet, e-MoS_2 nanosheet and MoS_2 powder based micro-supercapacitors at the current density of 0.22 Am^{-2}. Comparisons of the (C) specific gravimetric capacitance and (D) volumetric capacitance of h-MoS_2 nanosheet, e-MoS_2 nanosheet and MoS_2 powder based micro-supercapacitors at various scan rates.

3. Conclusion

In summary, we have demonstrated a simple and scalable approach to fabricate film based micro-supercapacitors via spray painting of MoS_2 nanosheets and subsequent laser patterning. The optimized MoS_2 film based micro-supercapacitor exhibits high area (8 mF cm^{-2}) and volumetric capacitances as well as excellent cycle performance, superior to EDLC-based micro-supercapacitors. Such efficient approach provides a good opportunity to develop various micro/nanosized energy storage devices to satisfy the requirements of portable, flexible, and transparent microelectronic devices.

4. Experimental Section

Hydrothermal Method-Produced h-MoS_2 Nanosheets: 10 mmol MoO_3, 25 mmol potassium thiocyanate and 64mg sodium dodecyl sulfate (SDS) were put into a Teflon-lined autoclave of 40 mL capacity, then, filled with 30 mL deionized water and sonicated for 30 min. The autoclave was sealed into a stainless steel tank and kept at 220 °C for 24 h, and then cooled to room temperature naturally. A dark powder was collected and washed with plenty of deionized water and ethanol several times to remove the residue of the reactants and surfactant. The remaining mixture is centrifuged and collected by vacuum filtration through a 0.45 μm PVDF filter membrane. The resulting solid is dried in vacuum oven at 90 °C overnight.

Liquid Exfoliation-Produced MoS_2 Nanosheets: Molybdenum disulfide powder was dissolved in DMF solvent and sonicated for 10 h (keep the water in sonicator cold). Centrifugation at 6000 rpm for 30 min was carried out and the supernatant was washed using ethanol and collected by pipette.

Characterization: Scanning electron microscopy (SEM) images were obtained on a high-resolution field-emission scanning electron microscope (FEI Quanta 400), the SEM samples were dissolved in ethanol and ultrasonicated for 30 min, following that dropped on a Si substrate for SEM testing. The TEM image and the selected area electron diffraction pattern were obtained on a JEOL 2100 Field Emission Gun TEM, the sample preparation process was similar to the one for SEM, but use the Cu grid with carbon supported instead of silicn substrate. XPS analyses were carried out on a PHI Quantera x-ray photoelectron spectrometer with a chamber pressure of 5×10^{-9} torr and an Al cathode as the X-ray source. The source power was set at 100 W, and pass energies of 140.00 eV for survey scans and 26.00 eV for high-resolution scans were used. Raman spectra were recorded with a Renishaw InVia Raman microscope using a 50x objective lens at room temperature, with a 514.5 nm laser beam and 1800 lines per mm grating. The Raman band of Si at 521 cm^{-1} was used as a reference to calibrate the spectrometer. XRD data was collected on a Rigaku D/Max Ultima α Powder X-ray diffractometer, sample was put inside the zero background sample holder during the testing.

Supporting Information

Supporting Information is available from the Wiley Online Library or from the author.

Acknowledgements

This work was financially supported by the US Army Research Office through a MURI grant (W911NF-11-1-0362) on Novel Free-Standing 2D Crystalline Materials focusing on Atomic Layers of Nitrides, Oxides, and Sulfides.

[1] J. H. Sung, S. J. Kim, S. H. Jeong, E. H. Kim, K. H. Lee, *J. Power Sources* **2006**, *162*, 1467–1470.
[2] H. K. Kim, S. H. Choi, Y. S. Yoon, S. Y. Chang, Y. W. Ok, T. Y. Seong, *Thin Solid Films* **2005**, *475*, 54–57.
[3] B. E. Conway, *J. Electrochem. Soc.* **1991**, *138*, 1539–1548.
[4] G. A. Snook, P. Kao, A. S. Best, *J. Power Sources* **2011**, *196*, 1–12.
[5] J. Wang, J. Polleux, J. Lim, B. Dunn, *J. Phys. Chem. C* **2007**, *111*, 14925–14931.
[6] J. Chmiola, C. Largeot, P. L. Taberna, P. Simon, Y. Gogotsi, *Science* **2010**, *328*, 480–483.
[7] D. Pech, M. Brunet, P. L. Taberna, P. Simon, N. Fabre, F. Mesnilgrente, V. Conedera, H. Durou, *J. Power Sources* **2010**, *195*, 1266–1269.
[8] D. Pech, M. Brunet, H. Durou, P. H. Huang, V. Mochalin, Y. Gogotsi, P. L. Taberna, P. Simon, *Nat. Nanotechnol.* **2010**, *5*, 651–654.
[9] V. L. Pushparaj, M. M. Shaijumon, A. Kumar, S. Murugesan, L. Ci, R. Vajtai, R. J. Linhardt, O. Nalamasu, P. M. Ajayan, *Proc. Natl. Acad. Sci. USA* **2007**, *104*, 13574–13577.
[10] S. W. Lee, B. S. Kim, S. Chen, Y. Shao-Horn, P. T. Hammond, *J. Am. Chem. Soc.* **2009**, *131*, 671–679.
[11] M. Kaempgen, C. K. Chan, J. Ma, Y. Cui, G. Gruner, *Nano Lett.* **2009**, *9*, 1872–1876.
[12] W. Gao, N. Singh, L. Song, Z. Liu, A. L. M. Reddy, L. J. Ci, R. Vajtai, Q. Zhang, B. Q. Wei, P. M. Ajayan, *Nat. Nanotechnol.* **2011**, *6*, 496–500.
[13] M. F. El-Kady, V. Strong, S. Dubin, R. B. Kaner, *Science* **2012**, *335*, 1326–1330.
[14] Y. W. Zhu, S. Murali, W. W. Cai, J. W. Suk, J. R. Potts, R. S. Ruoff, *Adv. Mater.* **2010**, *22*, 3906–3924.
[15] Y. W. Zhu, S. Murali, M. D. Stoller, K. J. Ganesh, W. W. Cai, P. J. Ferreira, A. Pirkle, R. M. Wallace, K. A. Cychosez, M. Thommes, D. Su, E. A. Stach, R. S. Ruoff, *Science* **2011**, *332*, 1537–1541.
[16] B. Radisavljevic, A. Radenovic, J. Brivio, V. Giacometti, A. Kis, *Nat. Nanotechnol.* **2011**, *6*, 147–150.
[17] B. Radisavljevic, M. B. Whitwick, A. Kis, *ACS Nano* **2011**, 5, 9934–9938.
[18] S. Bertolazzi, J. Brivio, A. Kis, *ACS Nano* **2011**, *5*, 9703–9709.
[19] D. J. Late, B. Liu, H. S. S. R. Matte, V. P. Dravid, C. N. R. Rao, *ACS Nano* **2012**, *6*, 5635–5641.
[20] Y. Y. Peng, Z. Y. Meng, C. Zhong, J. Lu, W. C. Yu, Y. B. Jia, Y. T. Qian, *Chem. Lett.* **2001**, *8*, 772–773.
[21] C. N. R. Rao, A. Nag, *Eur. J. Inorg. Chem.* **2010**, *27*, 4244–4250.
[22] H. S. S. R. Matte, A. Gomathi, A. K. Manna, R. Datta, S. K. Pati, C. N. R. Rao, *Angew. Chem., Int. Ed.* **2010**, *49*, 4059–4062.
[23] J. N. Coleman, M. Lotya, A. O'Neill, S. D. Bergin, P. J. King, U. Khan, K. Young, A. Gaucher, S. De, R. J. Smith, I. V. Shvets, S. K. Arora, G. Stanton, H. Y. Kim, K. Lee, G. T. Kim, G. S. Duesberg, T. Hallam, J. J. Boland, J. J. Wang, J. F. Donegan, J. C. Grunlan, G. Moriarty, A. Shmeliov, R. J. Nicholls, J. M. Perkins, E. M. Grieveson, K. Theuwissen, D. W. McComb, P. D. Nellist, V. Nicolosi, *Science* **2011**, *331*, 568–571.
[24] R. J. Smith, P. J. King, M. Lotya, C. Wirtz, U. Khan, S. De, A. O'Neill, G. S. Duesberg, J. C. Grunlan, G. Moriarty, J. Chen, J. Z. Wang, A. I. Minett, V. Nicolosi, J. N. Coleman, *Adv. Mater.* **2011**, *23*, 3944.
[25] J. M. Soon, K. P. Loh, *Electrochem. Solid-State Lett.* **2007**, *10*, A250–A254.
[26] B. E. Conway, *Electrochim. Acta* **1993**, *38*, 1249–1258.
[27] T. Brezesinski, J. Wang, S. H. Tolbert, B. Dunn, *Nat. Mater.* **2010**, *9*, 146–151.
[28] M. Zukalova, M. Kalbac, L. Kavan, I. Exnar, M. Graetzel, *Chem. Mater.* **2005**, *17*, 1248–1255.
[29] Z. Y. Yin, H. Li, H. Li, L. Jiang, Y. M. Shi, Y. H. Sun, G. Lu, Q. Zhang, X. D. Chen, H. Zhang, *ACS Nano* **2012**, *6*, 74–80.
[30] Z. Y. Zeng, Z. Y. Yin, X. Huang, H. Li, Q. Y. He, G. Lu, F. Boey, H. Zhang, *Angew. Chem., Int. Ed.* **2011**, *50*, 11093–11097.
[31] K. K. Liu, W. J. Zhang, Y. H. Lee, Y. C. Lin, M. T. Chang, C. Su, C. S. Chang, H. Li, Y. M. Shi, H. Zhang, C. S. Lai, L. J. Li, *Nano Lett.* **2012**, *12*, 1538–1544.
[32] H. Li, Z. Y. Yin, Q. Y. He, H. Li, X. Huang, G. Lu, D. W. H. Fam, A. I. Y. Tok, Q. Zhang, H. Zhang, *Small* **2012**, *8*, 63–67.
[33] Q. Y. He, Z. Y. Zeng, Z. Y. Yin, H. Li, S. X. Wu, X. Huang, H. Zhang, *Small* **2012**, *8*, 2994–2999.
[34] J. Q. Liu, Z. Y. Zeng, X. H. Cao, G. Lu, L. H. Wang, Q. L. Fan, W. Huang, H. Zhang, *Small* **2012**, *8*, 3517–3522.
[35] W. J. Zhou, Z. Y. Yin, Y. P. Du, X. Huang, Z. Y. Zeng, Z. X. Fan, H. Liu, J. Y. Wang, H. Zhang, *Small* **2013**, *9*, 140–147.

Received: December 17, 2012
Revised: January 21, 2013
Published online: April 16, 2013